2011 50th IEEE Conference on Decision and Control and
European Control Conference (CDC-ECC)
Orlando, FL, USA, December 12-15, 2011

Stability and Performance Analysis of Dual-Random-Rate Systems via Markov Jump Linear System Theory

Arturo Tejada, Jorge R. Chávez-Fuentes, and Pauline Vos

***Abstract*— This paper introduces the class of dual-random-rate systems (i.e., dual-rate systems with random output rates), which is well suited to model image-based control systems. It is shown that a dual-random-rate system can be reformulated as a switched linear system with a (quasi-periodic) random switching signal that is a static function of Markov chain. This reformulation makes it possible to study dual-random-rate systems with the stability and output performance analysis tools developed for Markov jump linear systems. The approach is illustrated via a practical example: the compensation of image drift in a transmission electron microscope.**

I. Introduction

Over the past 20 years, new control applications have emerged where computer vision or image-based sensors are used to control variables of interest. These applications range from robot or industrial process control [1]–[3], to biology [4], medicine [5], and microscopy [6], [7]. A common property of these so-called image-based control systems is that, due to the need of acquiring and processing images for feedback purposes, their sensing (or measurement) rates are generally slower than their actuation rates. This property allows one to analyze and design image-based control systems using multirate system theory [8], [9]. Multirate systems are generally analyzed under the assumption that their input and output rates are constant. In several image-based control systems, however, this assumption does not hold. For instance, image-based control can be used in a transmission electron microscope to regulate its optical properties [10]. However, not every image produce by the microscope can be used for control purposes (some must be used for scientific purposes). Moreover, the image acquisition and processing time can vary depending on the type of image being acquired (e.g., some images require longer acquisition times to ensure higher signal-to-noise ratios [11]). Thus, the rate of output data available for feedback purposes is not constant, and it is better described by a random variable of finite range. Thus, image-based control in a transmission electron microscope (and similar applications) is better represented by a multirate system with random output rates. However, to the best of our knowledge, such systems have not been studied in the literature yet.

This paper presents the initial steps towards a theory of multirate systems with random output rates. The analysis is restricted to the subclass of single-input, single-output linear dual-rate systems with random output rates, called here dual-random-rate systems, since these are the simplest subclass of multirate systems (see [12], [13] for information on dual-rate sytems). The analysis is based on the connection between dual-rate systems and periodic switched linear systems [14]. It is shown that a dual-random-rate system can be reformulated as a switched linear system with a (quasi-periodic) random switching signal that, under certain conditions, can be shown to be a static function of a Markov chain. This connection makes it possible to study dual-random-rate systems with tools developed for Markov jump linear systems (MJLSs) [15], [16].

A. Tejada and P. Vos are with the Delft Center for Systems and Control, Delft University of Technology, The Netherlands. Emails: {a.tejadaruiz, p.vos}@tudelft.nl

J. R. Chávez-Fuentes is with the Department of Mathematics, Pontificia Universidad Católica del Perú Email: jrchavez@pucp.edu.pe

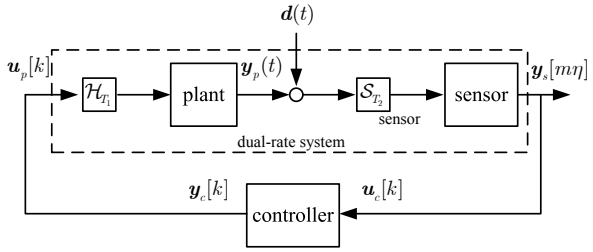

Fig. 1. Dual-rate, sampled-data, closed-loop control system. The sensing rate, T_2, is assumed to be η times slower than actuation rate, T_1 (i.e., $T_2 = \eta T_1$).

The rest of the paper is organized as follows: Section II presents the basics on dual-rate systems, shows their connection with switched linear systems and introduces the class of dual-random-rate systems. Section III summarizes the standard stability and output performance analysis tools for MJLS and relates them to dual-random-rate systems. Section IV presents an illustrative example, the compensation of image drift in a transmission electron microscope, while Section V presents our conclusions.

II. Dual-Random-Rate Systems

This section is divided in three parts. The first one provides the basic definition of a dual-rate system taking into account two types of output sensors: delayed and sporadic (see Figure 1). The second part provides dynamical models for such sensors and reformulates dual-rate systems as periodic switched linear systems. Finally, the last part introduces dual-random-rate systems, and shows that they can be reformulated as switched linear systems with a specific type of random switching signal.

In the sequel, $\mathbb{N}$ and $\mathbb{R}^+$ denote, respectively, the positive integers and the non-negative real numbers; random variables and processes are defined with respect to the probability space $(\Omega, \mathcal{F}, \Pr)$ and denoted with boldface fonts; and $\mathbf{E}\{\cdot\}$ denotes expectation.

A. Dual-Rate Systems

Consider the sampled-data, closed-loop control system shown in Figure 1. It is composed of a discrete-time controller in feedback interconnection with a linear continuous-time plant that is equipped with a "fast" actuator and a

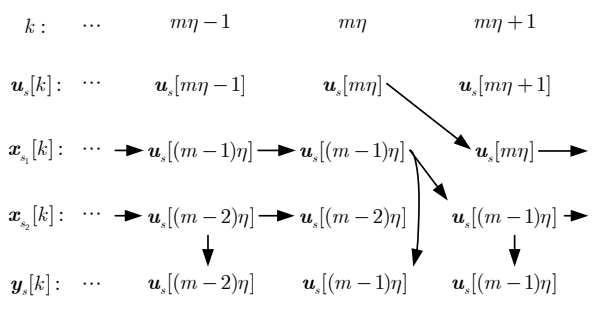

Fig. 2. Input, state, and output sequences of a delayed sensor.

"slow" sensor. More precisely, the controller drives the plant through an ideal hold operator, $\mathcal{H}_{T_1}$, with hold period T_1, while the plant's output, $\boldsymbol{y}_p(t)$, $t \in \mathbb{R}^+$, is measured by an ideal sensor equipped with a sample operator, $\mathcal{S}_{T_2}$, with sample period $T_2 \geq T_1$. For simplicity, it is assumed that $T_2 = \eta T_1$, $1\eta \in \mathbb{N}$, and that the sample and hold operators are synchronized. Thus, from the controller's perspective, the plant dynamics are discretized at the hold's rate and represented by

$$\begin{aligned} \boldsymbol{x}_p[k+1] &= A_p \boldsymbol{x}[k] + B_p \boldsymbol{u}_p[k] \\ \boldsymbol{y}_p[k] &= C_p \boldsymbol{x}_p[k] + D_p \boldsymbol{u}_p[k], \end{aligned} \tag{1}$$

where $k = 0, 1, \ldots$, $\boldsymbol{x}_p[k] \in \mathbb{R}^{n_p}$, $\boldsymbol{y}_p[k], \boldsymbol{u}_p[k] \in \mathbb{R}$, and A_p, B_p, C_p, and D_p are matrices of appropriate dimensions. On the other hand, the sensor provides the controller with a delayed-and-down-sampled or a down-sampled version of $\boldsymbol{y}_p[k]$, depending on the sensor type. More specifically, the sensor output at $k = m\eta$, $m = 0, 1, \ldots$, is given by

$$\text{Delayed: } \boldsymbol{y}_s[m\eta] = \boldsymbol{y}_p[(m-1)\eta] + \boldsymbol{d}[(m-1)\eta],^{1} \tag{2a}$$

$$\text{Sporadic: } \boldsymbol{y}_s[m\eta] = \boldsymbol{y}_p[m\eta] + \boldsymbol{d}[m\eta], \tag{2b}$$

where $\boldsymbol{d}[k] \in \mathbb{R}$, $k = 0, 1, \ldots$, denotes a random output perturbation process. A delayed sensor is one that does not produce instantaneous readouts of the plant output. That is, its dynamics are slower than plant's time constants (see e.g., [2], [12]). On the other hand, a sporadic sensor is one that has fast dynamics but can be used only infrequently compared to the plant's actuation rate (e.g., those used for image drift control [6]). This leads to the following definition (see also [12], [13]).

Definition 2.1: The system with input $\boldsymbol{u}_p[k]$ and output $\boldsymbol{y}_s[m\eta]$ described by (1)-(2) is called a **dual-rate system**.

Note that although $\boldsymbol{y}_s[k]$ is not defined for $k = m\eta + 1, \ldots, (m+1)\eta - 1$, it is needed for control law calculations for all $k = 0, 1, \ldots$. Although several strategies can be used to solve this problem [13], it is assumed here that the sensor's output is held constant between measurements. That is,

$$\boldsymbol{y}_s[k] \triangleq \boldsymbol{y}_s[m\eta], \tag{3}$$

for $k = m\eta + 1, \ldots, (m+1)\eta - 1$. This piecewise constant extension of $\boldsymbol{y}_s[m\eta]$ allows one to derive a joint switched dynamical model for the plant and the sensor as shown next.

B. Sensor Model and Switched System Representation

It follows from (2) and (3) that the sensor must posses internal memory in order to generate a piecewise constant output. Thus, from a modeling perspective, the sensor can be considered a dynamical system, with input $\boldsymbol{u}_s[k]$ and output $\boldsymbol{y}_s[k]$, that operates under two regimes: one while $\boldsymbol{y}_s[k]$ is held constant and another while $\boldsymbol{y}_s[k]$ is updated.

Consider first the case of a delayed sensor and let $\boldsymbol{u}_s[k] = \boldsymbol{y}_p[k] + \boldsymbol{d}[k]$ (i.e., assume there is an ideal sampler, with sample period T_1, between the summation node and $\mathcal{S}_{T_2}$ in Figure 1). It follows from equations (2a) and (3) that $\boldsymbol{y}_s[k] = \boldsymbol{u}_s[(m-1)\eta]$, $k = m\eta, \ldots, (m+1)\eta - 1$, $m = 0, 1, \ldots$. Thus, as shown in Figure 2, two internal states, $\boldsymbol{x}_{s_1}[k]$ and $\boldsymbol{x}_{s_2}[k]$, are needed to, respectively, down-sample $\boldsymbol{u}_s[k]$ and hold $\boldsymbol{y}_s[k]$ constant. The information flow among the sensor's input, states, and output is indicated by arrows in Figure 2. As needed, $\boldsymbol{y}_s[k] = \boldsymbol{u}_s[(m-1)\eta]$ when $k = m\eta$. Note that $\boldsymbol{u}_s[(m-1)\eta]$ is assumed to be stored in $\boldsymbol{x}_{s_1}[k]$, since it is not available from the input at time $k = m\eta$. Thus, $\boldsymbol{u}_s[k]$ must be stored in $\boldsymbol{x}_{s_1}[k]$ every $m\eta$ sample periods. Also, when $k = m\eta$, $\boldsymbol{x}_{s_1}[k]$ must be copied into $\boldsymbol{x}_{s_2}[k]$ to allow for $\boldsymbol{y}_s[k] = \boldsymbol{u}_s[(m-1)\eta]$ (i.e., $y_s[k] = \boldsymbol{x}_{s_2}[k]$) when $k = m\eta + 1, \ldots, (m+1)\eta - 1$. Finally, when $k = m\eta + 1, \ldots, (m+1)\eta$, $\boldsymbol{x}_{s_1}[k]$ and $\boldsymbol{x}_{s_2}[k]$ are held constant. Thus, a delayed sensor can be modeled as a switched linear system with state $\boldsymbol{x}_s[k] \triangleq [\boldsymbol{x}_{s_1}^{\mathrm{T}}[k]\ \boldsymbol{x}_{s_2}^{\mathrm{T}}[k]]^{\mathrm{T}} \in \mathbb{R}^{n_s}$, with $n_s = 2$, and dynamics given by

$$\begin{aligned} \boldsymbol{x}_s[k+1] &= A_{s_{\theta[k]}} \boldsymbol{x}_s[k] + B_{s_{\theta[k]}} \boldsymbol{u}_s[k] \\ \boldsymbol{y}_s[k] &= C_{s_{\theta[k]}} \boldsymbol{x}_s[k] + D_{s_{\theta[k]}} \boldsymbol{u}_s[k], \end{aligned} \tag{4}$$

where $\theta[k]$ is the periodic switching signal given by

$$\theta[k] = \begin{cases} 1, & k = m\eta, m = 0, 1, \ldots \\ 2, & \text{otherwise,} \end{cases} \tag{5}$$

and

$$\begin{aligned} A_{s_1}, B_{s_1}, C_{s_1}, D_{s_1} &= \left[\begin{smallmatrix} 0 & 0 \\ 1 & 0 \end{smallmatrix}\right], \left[\begin{smallmatrix} 1 \\ 0 \end{smallmatrix}\right], \left[\begin{smallmatrix} 1 & 0 \end{smallmatrix}\right], 0 \\ A_{s_2}, B_{s_2}, C_{s_2}, D_{s_2} &= \left[\begin{smallmatrix} 1 & 0 \\ 0 & 1 \end{smallmatrix}\right], \left[\begin{smallmatrix} 0 \\ 0 \end{smallmatrix}\right], \left[\begin{smallmatrix} 0 & 1 \end{smallmatrix}\right], 0. \end{aligned} \tag{6}$$

In the case of a sporadic sensor, a similar reasoning shows that the sensor can still be modeled by the periodic switched system in (4)-(5) provided that $\boldsymbol{x}_s[k]$ is simplified to a single state variable (i.e., $n_s = 1$) and that (6) is replaced by

$$\begin{aligned} A_{s_1}, B_{s_1}, C_{s_1}, D_{s_1} &= 0, 1, 0, 1 \\ A_{s_2}, B_{s_2}, C_{s_2}, D_{s_2} &= 1, 0, 1, 0. \end{aligned} \tag{7}$$

Finally, to derive a compact representation for the plant and the sensor, it will be assumed that $\boldsymbol{d}[k]$, $k = 0, 1, \ldots$, is a zero-mean, stationary random process. Consequently, $\boldsymbol{d}[k]$ can be assumed to be the output of a linear system driven by a scalar, zero-mean, independent and identically distributed (i.i.d.) process $\boldsymbol{w}[k]$, $k = 0, 1, \ldots$ [17]. That is,

$$\begin{aligned} \boldsymbol{x}_d[k+1] &= A_d \boldsymbol{x}_d[k] + B_d \boldsymbol{w}[k] \\ \boldsymbol{d}[k] &= C_d \boldsymbol{x}_d[k] + D_d \boldsymbol{w}[k], \end{aligned} \tag{8}$$

where $\boldsymbol{x}_d[k] \in \mathbb{R}^{n_d}$. Combining this equation with (1)-(5) yields the desired compact representation:

$$\begin{aligned} \boldsymbol{x}[k+1] &= A_{\theta[k]} \boldsymbol{x}[k] + B_{\theta[k]} \boldsymbol{u}_p[k] + G_{\theta[k]} \boldsymbol{w}[k] \\ \boldsymbol{y}[k] &= C_{\theta[k]} \boldsymbol{x}[k] + D_{\theta[k]} \boldsymbol{u}_p[k] + F_{\theta[k]} \boldsymbol{w}[k], \end{aligned} \tag{9}$$

where $\boldsymbol{x}[k] \triangleq [\boldsymbol{x}_p^{\mathrm{T}}[k]\ \boldsymbol{x}_d^{\mathrm{T}}[k]\ \boldsymbol{x}_s^{\mathrm{T}}[k]]^{\mathrm{T}}$, $\theta[k]$ is given by (5), and

$$A_{\theta[k]} = \begin{bmatrix} A_p & 0 & 0 \\ 0 & A_d & 0 \\ B_{s_{\theta[k]}} C_p & B_{s_{\theta[k]}} C_d & A_{s_{\theta[k]}} \end{bmatrix}, \quad B_{\theta[k]} = \begin{bmatrix} B_p \\ 0 \\ B_{s_{\theta[k]}} D_p \end{bmatrix},$$

[1] $\boldsymbol{y}_s[0]$ is set to an arbitrary value.

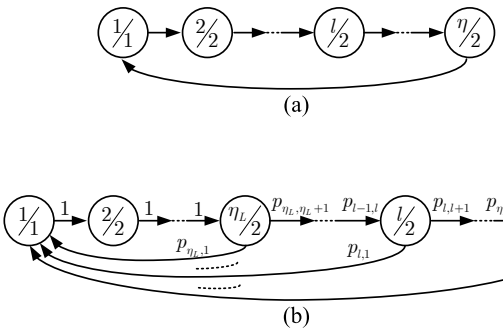

Fig. 3. (a) Autonomous, time-driven, deterministic automaton that generates $\theta[k]$ in (5). (b) State transition diagram of the Markov chain $\tilde{\boldsymbol{\theta}}[k]$ that generates $\boldsymbol{\theta}[k]$ in (11). The states are labeled with the standard $\cdot/\cdot$ notation denoting the state/output values. In (b), each arrow is labeled with a transition probability value.

$$C_{\theta[k]} = \left[\, {}^{D_{s_{\theta[k]}}C_p} \;\; {}^{D_{s_{\theta[k]}}C_d} \;\; C_{s_{\theta[k]}} \,\right], \qquad D_{\theta[k]} = D_{s_{\theta[k]}} D_p,$$

$$F_{\theta[k]} = D_{s_{\theta[k]}} D_d, \qquad G_{\theta[k]} = \begin{bmatrix} 0 \\ B_d \\ B_{s_{\theta[k]}} D_d \end{bmatrix}.$$

Throughout this subsection η has been considered fixed. In many practical situations, however, η may vary randomly, which motivates the analysis presented next.

C. Dual-Random-Rate Systems

In the previous subsection it was shown that a dual-rate system can be reformulated as a linear switched system driven by a periodic switching signal $\theta[k]$. The latter can be considered to be generated by an autonomous, time-driven, deterministic automaton with state $\tilde{\theta}[k] \in \{1, \ldots, \eta\}$, initial state $\tilde{\theta}[0] = 1$[2], output map $\varpi : \{1, \ldots, \eta\} \to \{1, 2\}$

$$\varpi : \tilde{\theta}[k] \mapsto \theta[k] = \varpi(z[k]) = \begin{cases} 1, & \tilde{\theta}[k] = 1, \\ 2, & \tilde{\theta}[k] \neq 1 \end{cases}, \qquad (10)$$

and state transition diagram given in Figure 3(a). Clearly, each cycle of $\theta[k]$ lasts exactly η sample periods. In many practical situations, however, each cycle's duration may be shorter or longer than η sample periods. For instance, the time it takes an image-based sensor to generate a new output may vary depending on the amount of processing time that each particular image needs. Similarly, in a networked control system, the time it takes new sensor data to reach the controller varies depending on the network's level of congestion [18]. In such cases, each cycles' duration can be considered a random variable with an *average* value of η sample periods. Thus, let $\boldsymbol{\eta}_m \in \{\eta_L, \ldots, \eta_H\}$, with $\eta_L, \eta_H \in \mathbb{N}$ and $\eta_L \leq \eta_h$, denote m-th cycle's duration and, for simplicity, assume that all $\boldsymbol{\eta}_m$, $m = 0, 1, \ldots$ are i.i.d. with probability distribution, $\mu \triangleq [\mu_{\eta_L}, \ldots, \mu_{\eta_H}]$, with $\mu_i = \Pr\{\boldsymbol{\eta}_m = i\}$, $i = \eta_L, \ldots, \eta_H$, $m = 1, 2, \ldots$. Clearly, under these conditions, the switching signal becomes the random process, $\boldsymbol{\theta}[k]$, $k = 0, 1, \ldots$, given by

$$\boldsymbol{\theta}[k] = \begin{cases} 1, & k = 0, \boldsymbol{\eta}_1, \boldsymbol{\eta}_1 + \boldsymbol{\eta}_2, \cdots \\ 2, & \text{otherwise} \end{cases}. \qquad (11)$$

[2]Note that $\tilde{\theta}[0]$ is set to 1 to make $\theta[0] = 1$. This, however, was only needed to simplify the derivation of (4). Thus, in general, $\tilde{\theta}[0]$ can take any value from the set $\{1, \ldots, \eta\}$.

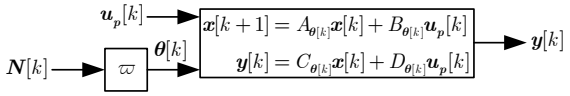

Fig. 4. Alternative representation for a dual-random-rate system.

Moreover, if $\boldsymbol{\theta}[k] = 1$ for some $k \geq 0$ then

$$\Pr\{\boldsymbol{\theta}[k+i] = 1 \big| \boldsymbol{\theta}[k] = 1\} = \begin{cases} \mu_i, & i = \eta_L, \ldots, \eta_H, \\ 0, & \text{otherwise} \end{cases}. \qquad (12)$$

This leads to the following definition.

Definition 2.2: The switched system (9) switched by the signal $\boldsymbol{\theta}[k]$ in (11)-(12) is called a **dual-random-rate system** and denoted $\mathfrak{D}$.

Observe from (11) and (12) that $\boldsymbol{\theta}[k]$ can be generated by applying the map ϖ in (10), with extended domain $\{1, \ldots, \eta_H\}$, to an η_H-states homogeneous Markov chain $\tilde{\boldsymbol{\theta}}[k]$, $k = 0, 1, \ldots$, with state transition diagram given by Figure 3(b), initial distribution[3] $\mu_0^{\tilde{\theta}} \triangleq [\mu_{0_1}^{\tilde{\theta}} \;\; \ldots \;\; \mu_{0_{\eta_H}}^{\tilde{\theta}}]$, and transition probability matrix $\Pi = [\pi_{i,j}]$ with transition probabilities

$$\pi_{i,j} = \begin{cases} 1, & i = 1, \ldots, \eta_L - 1, j = i + 1, \\ \dfrac{\mu_i}{\sum_{l=i}^{\eta_H} \mu_l}, & i = \eta_L, \ldots, \eta_H, j = 1, \\ 1 - \pi_{i,1}, & i = \eta_L, \ldots, \eta_H, j = i + 1 \end{cases}. \qquad (13)$$

Thus, $\mathfrak{D}$ can be considered to be a switched linear system switched by a static function of a Markov chain (see Figure 4), so its stability and performance properties can be established using tools available for MJLSs, as shown next.

III. Stability and Performance Analysis of Dual-Random-Rate Systems

This section is divided into two parts. The first part summarizes well-known results on the stability and output performance of MJLSs. The second part relates these results to dual-random-rate systems.

A. Stability and Output Performance of MJLS

Consider the Markov jump linear system

$$\begin{aligned} \tilde{\boldsymbol{x}}[k+1] &= \tilde{A}_{\tilde{\boldsymbol{\theta}}[k]} \tilde{\boldsymbol{x}}[k] + \tilde{B}_{\tilde{\boldsymbol{\theta}}[k]} \boldsymbol{u}[k] + \tilde{G}_{\tilde{\boldsymbol{\theta}}[k]} \boldsymbol{w}[k] \\ \tilde{\boldsymbol{y}}[k] &= \tilde{C}_{\tilde{\boldsymbol{\theta}}[k]} \tilde{\boldsymbol{x}}[k] + \tilde{D}_{\tilde{\boldsymbol{\theta}}[k]} \boldsymbol{u}[k] + \tilde{F}_{\tilde{\boldsymbol{\theta}}[k]} \boldsymbol{w}[k] \end{aligned}, \qquad (14)$$

where, $\tilde{\boldsymbol{x}}[k] \in \mathbb{R}^n$, $\tilde{\boldsymbol{x}}[0]$ is a second-order random vector, $\tilde{\boldsymbol{y}}[k], \boldsymbol{u}[k] \in \mathbb{R}$, $\boldsymbol{w}[k]$ is the i.i.d. process in (8), and $\tilde{\boldsymbol{\theta}}[k]$, $k = 0, 1, \ldots$, is the Markov chain defined in (13).

Note that by construction, the states of $\tilde{\boldsymbol{\theta}}[k]$ constitute a single recurrent class but are not necessarily aperiodic [19]. However, aperiodicity can be guaranteed by imposing mild additional conditions on $\tilde{\boldsymbol{\theta}}[k]$, $k = 0, 1, \ldots$, (e.g., $\pi_{i,1} > 0$ and $\pi_{i+1,1} > 0$ for some $i \in \{\eta_L, \ldots, \eta_H - 1\}$). Thus, it will be assumed in the sequel that $\tilde{\boldsymbol{\theta}}[k]$, $k = 0, 1, \ldots$, is aperiodic and, thus, ergodic [19] (as required by Theorems 3.1 to 3.3).

The stability notion of choice for a MJLS, mean square stability (MSS), is defined next [15], [20].

Definition 3.1: The MJLS (14) with $\boldsymbol{u}[k] \equiv 0$ and $\boldsymbol{w}[k] \equiv 0$ is said to be **mean square stable** if for every initial

[3]As in the previous subsection, $\tilde{\boldsymbol{\theta}}[0]$ must not necessarily be set to 1.

distribution $\mu_0^{\tilde{\theta}}$ and every initial state vector, $\tilde{x}_0$, it follows that $\mathbf{E}\{\|\tilde{\boldsymbol{x}}[k]\|^2\} \to 0$ as $k \to \infty$.

MSS can be tested as follows (see [15, Theorem 3.9]).

Theorem 3.1: The MJLS (14) with $\boldsymbol{u}[k] \equiv 0$ and $\boldsymbol{w}[k] \equiv 0$ is mean square stable if and only if the spectral radius of $\mathcal{A}_2$, denoted $\rho(\mathcal{A}_2)$, is less than 1, where

$$\mathcal{A}_2 \triangleq (\tilde{A}_1^T \otimes \tilde{A}_1^T, \ldots, \tilde{A}_{\eta_H}^T \otimes \tilde{A}_{\eta_H}^T)(\Pi \otimes I_{n^2}) \tag{15}$$

and I_{n^2} is an $n^2 \times n^2$ identity matrix.

Different closed-loop controllers for MJLSs can compared using the following output performance measures [16], [21].

Definition 3.2: The **output performance measure** J for the MJLS (14) is given by

$$J = \begin{cases} J_0 \triangleq \mathbf{E}\left\{\sum_{k=0}^{\infty} ||\tilde{\boldsymbol{y}}[k]||^2\right\}, & \boldsymbol{w}[k] = 0, \\ J_w \triangleq \lim_{k\to\infty} \mathbf{E}\{||\tilde{\boldsymbol{y}}[k]||^2\}, & \boldsymbol{w}[k] \neq 0 \end{cases}$$

where J_0 is the *mean output energy* and J_w is the *mean output power*.

J_0 is a measure of how quickly the MJLS (14) dissipates energy at its output. To obtain a closed-form expression for it, let $\mathcal{C} \triangleq [\mathcal{C}_1 \ \ldots \ \mathcal{C}_{\eta_H}] \in \mathbb{R}^{n\times n\eta_H}$ and $\mathcal{Q} \triangleq [\mathcal{Q}_1 \ \ldots \ \mathcal{Q}_{\eta_H}] \in \mathbb{R}^{n\times n\eta_H}$, where $\mathcal{C}_j = \tilde{C}_j^{\mathrm{T}}\tilde{C}_j \in \mathbb{R}^{n\times n}$, $j = 1, \ldots, \eta_H$, and $\mathcal{Q}_i \in \mathbb{R}^{n\times n}$, $j = 1, \ldots, \eta_H$, are given by

$$\mathcal{Q} = \varphi^{-1}\left(\left(I_{n^2\eta_H} - \mathcal{A}_2\right)^{-1}\varphi(\mathcal{C})\right).$$

In this equation, $\mathcal{A}_2$ is defined as in (15), and the invertible function $\varphi : \mathbb{R}^{n\times n\eta_H} \to \mathbb{R}^{n^2\eta_H}$ has action $\varphi : \mathcal{C} \mapsto \varphi(\mathcal{C}) \triangleq [\mathrm{vec}^{\mathrm{T}}(\mathcal{C}_1) \ \ldots \mathrm{vec}^{\mathrm{T}}(\mathcal{C}_{\eta_H})]^{\mathrm{T}}$, where $\mathrm{vec}(\cdot)$ denotes the column stacking operator. J_0 can then be computed as follows.

Theorem 3.2 (Theorem 4.2 in [21]): Consider the MJLS (14) with $\boldsymbol{u}[k] \equiv 0$ and $\boldsymbol{w}[k] \equiv 0$ and assume it is MSS. If $\tilde{\boldsymbol{x}}[0]$ and $\tilde{\boldsymbol{\theta}}[k]$, $k = 0, 1, \ldots$, are independent, then

$$J_0 = \mathrm{tr}(X_0 Q_0),$$

where $X_0 \triangleq E\{\tilde{\boldsymbol{x}}(0)\tilde{\boldsymbol{x}}^{\mathrm{T}}(0)\}$ and $\mathcal{Q}_0 \triangleq \sum_{j=1}^{\eta_H} \mathcal{Q}_j \mu_{0_j}^{\tilde{\theta}}$.

J_w is a measure of how well the MJLS (14) rejects $\boldsymbol{w}[k]$. To derive a closed-from expression for it, first note from the ergodicity of $\tilde{\boldsymbol{\theta}}[k]$ that it has a unique steady state distribution $\mu_s^{\tilde{\theta}} \triangleq [\mu_{s_1}^{\tilde{\theta}} \ \ldots \ \mu_{s_{\eta_H}}^{\tilde{\theta}}]$. Next, let $\mathcal{V} \triangleq [\mathcal{V}_1 \ \ldots \ \mathcal{V}_{\eta_H}] \in \mathbb{R}^{n\times n\eta_H}$ and $\check{\mathcal{Q}} \triangleq [\check{\mathcal{Q}}_1 \ \ldots \ \check{\mathcal{Q}}_{\eta_H}] \in \mathbb{R}^{n\times n\eta_H}$, where $\mathcal{V}_j \triangleq \sum_{i=1}^{\eta_H} \pi_{i,j}\tilde{G}_i\tilde{G}_i^{\mathrm{T}}\mu_{s_i}^{\tilde{\theta}}$, $j = 1, \ldots, \eta_H$, and $\check{\mathcal{Q}}_j \in \mathbb{R}^{n\times n}$, $j = 1, \ldots, \eta_H$, are obtained from

$$\check{\mathcal{Q}} = \varphi^{-1}\left(\left(I_{n^2\eta_H} - \mathcal{A}_2^{\mathrm{T}}\right)^{-1}\varphi(\mathcal{V})\right).$$

J_w can be computed as follows.

Theorem 3.3: Consider the MJLS (14) with $\boldsymbol{u}[k] \equiv 0$ and $\sigma_w^2 = 1$, and assume it is MSS. If $\tilde{\boldsymbol{x}}[0]$, $\boldsymbol{w}[k]$, $k = 0, 1, \ldots$, and $\tilde{\boldsymbol{\theta}}[k]$, $k = 0, 1, \ldots$, are independent, then

$$J_w = \mathrm{tr}\left(\sum_{j=1}^{\eta_H} \mathcal{C}_j\check{\mathcal{Q}}_j\right) + \sum_{j=1}^{\eta_H} \tilde{F}_j^2\mu_{s_j}^{\tilde{\theta}}.$$

Proof: Since $\tilde{\boldsymbol{y}}[k]$ is scalar, it follows from (14) that $\mathbf{E}\{\|\tilde{\boldsymbol{y}}[k]\|^2\} = \mathbf{E}\{(\tilde{C}_{\tilde{\boldsymbol{\theta}}[k]}\tilde{\boldsymbol{x}}[k])^2 + 2\tilde{C}_{\tilde{\boldsymbol{\theta}}[k]}\tilde{\boldsymbol{x}}[k]\tilde{F}_{\tilde{\boldsymbol{\theta}}[k]}\boldsymbol{w}[k] + (\tilde{F}_{\tilde{\boldsymbol{\theta}}[k]}\boldsymbol{w}[k])^2\}$. Since, by assumption, $\tilde{\boldsymbol{x}}[k]$, $\tilde{\boldsymbol{\theta}}[k]$, and $\boldsymbol{w}[k]$ are independent, then it follows that $\mathbf{E}\{\|\tilde{\boldsymbol{y}}[k]\|^2\} = \mathbf{E}\{(\tilde{C}_{\tilde{\boldsymbol{\theta}}[k]}\tilde{\boldsymbol{x}}[k])^2\} + \sigma_w^2\mathbf{E}\{\tilde{F}_{\tilde{\boldsymbol{\theta}}[k]}^2\}$. The result follows immediately by taking the limit, when $k \to \infty$, of the latter equality and using [16, Theorem 9 and Corollary 8] and the ergodicity of $\tilde{\boldsymbol{\theta}}[k]$, $k = 0, 1, \ldots$. ∎

These results can be applied to dual-random-rate systems as shown next.

B. Stability and Performance of Dual-Random-Rate Systems

Consider again the dual-random-rate system $\mathfrak{D}$ and recall that $\boldsymbol{\theta}[k] = \varpi(\tilde{\boldsymbol{\theta}}[k])$. Next, in (14) set $\tilde{A}_i = A_{\varpi(i)}$, $\tilde{B}_i = B_{\varpi(i)}$, $\tilde{C}_i = C_{\varpi(i)}$, $\tilde{D}_i = D_{\varpi(i)}$, $\tilde{F}_i = F_{\varpi(i)}$, and $\tilde{G}_i = G_{\varpi(i)}$, for all $i = 1, \ldots, \eta_H$, where A_l, B_l, C_l, D_l, F_l, and G_l, $l = 1, 2$, are defined as in (9). Under such conditions, the MJLS in (14) is said to be *model equivalent* to the dual-random rate system $\mathfrak{D}$ [16]. That is, if $\tilde{\boldsymbol{x}}[0] \equiv \boldsymbol{x}[0]$ and $\boldsymbol{u}[k] \equiv \boldsymbol{u}_p[k]$ for all $k = 0, 1, \ldots$, then $\tilde{\boldsymbol{x}}[k] \equiv \boldsymbol{x}[k]$ and $\tilde{\boldsymbol{y}}[k] \equiv \boldsymbol{y}[k]$ for all $k = 0, 1, \ldots$. Moreover, both systems have equivalent stability and performance properties [16], [22]. Consequently, the stability and performance properties of $\mathfrak{D}$ can be established by analyzing those of its model equivalent MJLS (provided, of course, that $\boldsymbol{x}[0]$ is a second-order random vector, and that it, $\tilde{\boldsymbol{\theta}}[k], k = 0, 1, \ldots$, and $\boldsymbol{w}[k], k = 0, 1, \ldots$, are independent, which is usually the case in practice since the initial state, the output rate and the output perturbation are independent physical variables).

Note that in practical applications $\tilde{\boldsymbol{\theta}}[k]$ may be accesible as a signal (e.g., in electron microscopy). In such cases, the dual-random-rate system $\mathfrak{D}$ can be connected to a MJLS controller in a configuration similar to that in Figure 1. If the controller dynamics are given by

$$\begin{aligned} \boldsymbol{x}_c[k+1] &= A_{c_{\tilde{\boldsymbol{\theta}}[k]}}\boldsymbol{x}_c[k] + B_{c_{\tilde{\boldsymbol{\theta}}[k]}}\boldsymbol{y}_s[k] \\ \boldsymbol{y}_c[k] &= C_{c_{\tilde{\boldsymbol{\theta}}[k]}}\boldsymbol{x}_c[k], \end{aligned} \tag{16}$$

where $\boldsymbol{x}_c[k] \in \mathbb{R}^{n_c}$ and $\boldsymbol{y}_c[k] \in \mathbb{R}$, then the feedback interconnection between $\mathfrak{D}$ and the controller is given by

$$\begin{aligned} \boldsymbol{x}_{\mathrm{cl}}[k+1] &= A_{\mathrm{cl}_{\tilde{\boldsymbol{\theta}}[k]}}\boldsymbol{x}_{\mathrm{cl}}[k] + G_{\mathrm{cl}_{\tilde{\boldsymbol{\theta}}[k]}}\boldsymbol{w}[k] \\ \boldsymbol{y}_{\mathrm{cl}}[k] &= C_{\mathrm{cl}_{\tilde{\boldsymbol{\theta}}[k]}}\boldsymbol{x}_{\mathrm{cl}}[k] + F_{\mathrm{cl}_{\tilde{\boldsymbol{\theta}}[k]}}\boldsymbol{w}[k], \end{aligned} \tag{17}$$

where $\boldsymbol{x}_{\mathrm{cl}}[k] \triangleq \begin{bmatrix}\boldsymbol{x}_p^{\mathrm{T}}[k] & \boldsymbol{x}_d^{\mathrm{T}}[k] & \boldsymbol{x}_s^{\mathrm{T}}[k] & \boldsymbol{x}_c^{\mathrm{T}}[k]\end{bmatrix}^{\mathrm{T}}$ and $A_{\mathrm{cl}_{\tilde{\boldsymbol{\theta}}[k]}}$, $G_{\mathrm{cl}_{\tilde{\boldsymbol{\theta}}[k]}}$, $C_{\mathrm{cl}_{\tilde{\boldsymbol{\theta}}[k]}}$, and $F_{\mathrm{cl}_{\tilde{\boldsymbol{\theta}}[k]}}$ are given in (18) (top of next page). Note that $C_{\mathrm{cl}_{\tilde{\boldsymbol{\theta}}[k]}}$ was chosen so that $\boldsymbol{y}_{\mathrm{cl}}[k] = \boldsymbol{y}_p[k] + \boldsymbol{d}[k]$, for all $k = 0, 1, \ldots$, since this is the output signal of most interest. Finally, note that (17) is a particular case of (14) so it can be directly analyzed with the tools described in Section III.A. These concepts are illustrated next.

IV. Example

Transmission electron microscopes (TEMs) are the tools of choice for nanotechnology and biological research since they can reveal information on the internal structure of a wide range of specimens. Although currently, most of these microscopes are operated manually, it is expected that in the near future autonomous TEMs will be needed to perform high-throughput nano-measurements [23]. One aspect of TEM automation that requires special attention is that of image drift compensation (see, e.g., [24]). TEM images are generated by shining a beam of electron through a thin specimen. The beam is composed mostly of electrons that have a vertical downward trajectory. When the electrons interact with the specimen, they get scattered at angles that depend on the atomic weight of the elements composing

$$A_{\mathrm{cl}_{\tilde{\boldsymbol{\theta}}[k]}} = \begin{bmatrix} A_p & 0 & 0 & B_p C_{c_{\theta[k]}} \\ 0 & A_d & 0 & 0 \\ B_{s_{\theta[k]}} C_p & B_{s_{\theta[k]}} C_d & A_{s_{\theta[k]}} & B_{s_{\theta[k]}} D_p C_{c_{\theta[k]}} \\ B_{c_{\theta[k]}} D_{s_{\theta[k]}} C_p & B_{c_{\theta[k]}} D_{s_{\theta[k]}} C_d & B_{c_{\theta[k]}} C_{s_{\theta[k]}} & A_{c_{\theta[k]}} + B_{c_{\theta[k]}} D_{s_{\theta[k]}} D_p C_{c_{\theta[k]}} \end{bmatrix}, \quad G_{\mathrm{cl}_{\tilde{\boldsymbol{\theta}}[k]}} = \begin{bmatrix} 0 \\ B_d \\ B_{s_{\theta[k]}} D_d \\ B_{c_{\theta[k]}} D_{s_{\theta[k]}} D_d \end{bmatrix},$$
$$C_{\mathrm{cl}_{\tilde{\boldsymbol{\theta}}[k]}} = \begin{bmatrix} C_p & C_d & 0 & D_p C_{c_{\theta[k]}} \end{bmatrix}, \quad F_{\mathrm{cl}_{\tilde{\boldsymbol{\theta}}[k]}} = D_d. \tag{18}$$

the specimen. In general, heavier atoms scatter the electrons at higher angles than lighter atoms. Thus, by setting-up the TEM optical system to allow only slightly scattered or unscattered electrons to reach the microscope's viewing screen or CCD camera, it is possible to generate bright-field images that show dark spots only where the specimen contains heavier atoms [11]. Clearly, the image content depends on the relative position of the specimen and the beam. In practice, even if this relative position remains constant, the image content is known to drift due to external perturbations [25]. Image drift is corrected using shift-coils, which allow one to laterally displace the electrons that go through the specimen before they reach the CCD camera. In this way, one can shift the image content and counteract the drift. Several schemes have been proposed to automatically compensate image drift [6], [7]. These schemes assume that images can be acquired at regular intervals from which the drift can be estimated by image processing. The drift information is then used to stir the shift-coils appropriately. The aforementioned assumption, however, overlooks the fact that not all images can be used for drift control purposes, since some must be used for scientific purposes. More importantly, the sequence and/or the proportion of scientific images with respect to control images may vary randomly. Clearly, drift compensation can be characterized as a dual-random-rate system.

To illustrate this, assume that the position of the specimen is fixed and that the drift only acts in one direction (i.e., the drift is only a scalar). Let the plant in Figure 1 represent the shift-coils and note that $\boldsymbol{y}_p(t)$ represents in this case the desired image content position (in the same direction as the drift). The drift, $\boldsymbol{d}(t)$, is represented here as an additive perturbation to $\boldsymbol{y}_p(t)$. It can be estimated from the image stream by an image processing algorithm that compares each image against a reference image by using, for instance, cross correlation methods [6]. In practice, the shift-coils transients are much shorter than the drift time constants, so they can be treated as static systems with static gain K [24]. (Without loss of generality, it will be assumed that $K = 1$.) Thus, in (1), $A_p = 0$, $B_p = 0$, $C_p = 0$, $D_p = 1$. In this example, the drift is assumed to be a zero-mean ARMA(1,1) process, so in (8), $A_d = \phi$, $B_d = 1$, $C_d = \phi - \theta$, $D_d = 1$, with $\phi = -0.1$, $\theta = 0.9$ and $\sigma_w^2 = 1$ (see [26]). If one assumes that two scientific images are acquired every 9 control images in average (i.e., 90% of the time the image stream is used for control purposes), then the action of the CCD camera and the image processing algorithm can be modeled as a sporadic sensor (see (2b)) with dynamics (4), (7) driven by $\boldsymbol{\theta}[k]$ in (11)-(12), with $\eta_L = 1$, $\eta_H = 3$, $\mu_1 = 0.9$, $\mu_2 = 0$, and $\mu_3 = 0.1$. Thus, the transition probability matrix of $\tilde{\boldsymbol{\theta}}[k]$ in (13) is given by

$$\Pi = \begin{bmatrix} 0.9 & 0.1 & 0 \\ 0 & 0 & 1 \\ 1 & 0 & 0 \end{bmatrix}.$$

As suggested in [24], the controller will attempt to minimize the variance of the observed image drift by executing a minimum variance control (MVC) scheme [27]. This scheme makes use of drift estimates, $\hat{\boldsymbol{d}}[k]$, and an internal model of the drift dynamics to forecast the future drift values and compensate for them. More precisely, suppose that the k-th image is used for control purposes and that the $k+1$-th and $k+2$-th images are used for scientific purposes. After the k-th image is acquired (i.e., when $\tilde{\boldsymbol{\theta}}[k] = 1$), the output of the sensor is given by $\boldsymbol{y}_s[k] = \boldsymbol{y}_p[k] + \boldsymbol{d}[k] - y_{ref} - d_{ref}$, where $y_{ref} + d_{ref}$ is the position of the reference image content with respect to an absolute frame of spatial coordinates. If $y_{ref} + d_{ref}$ is assumed to be zero (see [24]), the drift can be estimated by computing $\hat{\boldsymbol{d}}[k] = \boldsymbol{y}_s[k] - K\boldsymbol{u}_p[k]$. Under the standard MVC scheme, $\boldsymbol{u}_p[k+1] = -\hat{\boldsymbol{d}}[k,1]$, where $\hat{\boldsymbol{d}}[k,1]$ is the forecast of $\boldsymbol{d}[k+1]$ produced with the information available up to the k-th image. When the scientific images are being acquired (i.e., when $\tilde{\boldsymbol{\theta}}[k+1] = 2$ and $\tilde{\boldsymbol{\theta}}[k+2] = 3$) the estimates $\hat{\boldsymbol{d}}[k+1]$ and $\hat{\boldsymbol{d}}[k+2]$ are no longer available. In such case, the two and three steps ahead forecasts, $\hat{\boldsymbol{d}}[k,2]$ and $\hat{\boldsymbol{d}}[k,3]$, are used to generate $\boldsymbol{u}_p[k+2]$ and $\boldsymbol{u}_p[k+3]$ respectively. (Note that the latter alternative is not part of the standard MVC scheme.) As shown in [26], the forecasts for image k can be related to those for image $k-1$ as follows

$$\begin{aligned} \hat{\boldsymbol{d}}[k,1] &= \hat{\boldsymbol{d}}[k-1,2] + \psi_1 \hat{\boldsymbol{w}}[k] \\ \hat{\boldsymbol{d}}[k,2] &= \hat{\boldsymbol{d}}[k-1,3] + \psi_2 \hat{\boldsymbol{w}}[k] \\ \hat{\boldsymbol{d}}[k,3] &= \phi \hat{\boldsymbol{d}}[k-1,3] + \psi_3 \hat{\boldsymbol{w}}[k], \end{aligned}$$

where $\psi_i = (\phi - \theta)\phi^{i-1}$, $i = 1, 2, 3$, and $\hat{\boldsymbol{w}}[k]$ an estimate of $\boldsymbol{w}[k]$ (which is not directly measurable) is given by $\hat{\boldsymbol{w}}[k] = \hat{\boldsymbol{d}}[k] - \phi\hat{\boldsymbol{d}}[k-1] + \theta\hat{\boldsymbol{w}}[k-1]$. Thus, if $\boldsymbol{x}_c[k] \triangleq [\boldsymbol{d}_1[k] \quad \boldsymbol{d}_2[k] \quad \boldsymbol{d}_3[k] \quad \boldsymbol{d}_m[k] \quad \boldsymbol{w}_m[k]]$, where $\boldsymbol{d}_1[k]$, $\boldsymbol{d}_2[k]$, and $\boldsymbol{d}_3[k]$ are used to store, respectively, $\hat{\boldsymbol{d}}[k,1]$, $\hat{\boldsymbol{d}}[k,2]$ and $\hat{\boldsymbol{d}}[k,3]$, $\boldsymbol{d}_m[k]$ stores $\boldsymbol{d}[k]$, and $\boldsymbol{w}_m[k]$ stores $\hat{\boldsymbol{w}}[k]$, then the controller can be represented as in (16) with matrices

$$A_{c_1} = \begin{bmatrix} \psi_1 & 1 & 0 & -\psi_1\phi & \psi_1\theta \\ \psi_2 & 0 & 1 & -\psi_2\phi & \psi_2\theta \\ \psi_3 & 0 & \phi & -\psi_3\phi & \psi_3\theta \\ 1 & 0 & 0 & 0 & 0 \\ 1 & 0 & 0 & -\phi & \theta \end{bmatrix}, A_{c_2} = A_{c_3} = I_5,$$

$B_{c_1} = [\psi_1 \quad \psi_2 \quad \psi_3 \quad 1 \quad 1]^{\mathrm{T}}$, $B_{c_2} = B_{c_3} = 0_{5\times 1}$, $C_{c_1} = [-1 \quad 0 \quad 0 \quad 0 \quad 0]$, $C_{c_2} = [0 \quad -1 \quad 0 \quad 0 \quad 0]$, and $C_{c_3} = [0 \quad 0 \quad -1 \quad 0 \quad 0]$, where I_5 is a 5×5 identity matrix, $0_{5\times 1}$ is a 5×1 column vector of zeros.

The stability of this extended MVC scheme can be analyzed by means of (17) and Theorem 3.1 (in this case, $\boldsymbol{x}_{\mathrm{cl}}[k] \in \mathbb{R}^8$). It is not difficult to show that $\mathcal{A}_2 = 0.8430 < 1$ (see (15)), so the extended MVC scheme is mean square stable. Also note from Theorems 3.2 and 3.3 that the mean output energy and the mean output power are, respectively, $J_0 = 120.9$ and $J_w = 90.86$. To confirm these results, two sets of Monte Carlo simulations were performed using Matlab. The first simulation set illustrates Theorem 3.2. It comprised 100000 sample paths of the closed-loop system (17), each of a length of 100 sample periods (i.e., k=0,1,...,99). The initial distribution of $\tilde{\boldsymbol{\theta}}[k]$ was set to

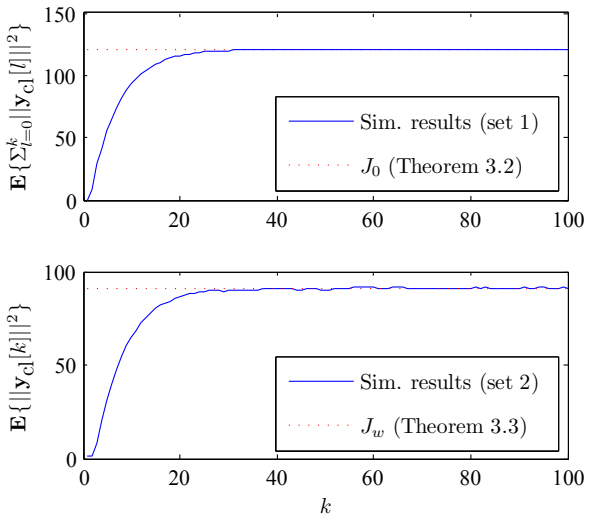

Fig. 5. Example simulation results (see Section IV). Top: Results of the first simulation set that show that, as expected, $\mathbf{E}\{\sum_{l=0}^{k}\|\boldsymbol{y}_{\mathrm{cl}}[l]\|^2\} \to J_0$ as $k \to \infty$. Bottom: Results of the second simulation that show that, as expected, $\mathbf{E}\{\|\boldsymbol{y}_{\mathrm{cl}}[k]\|^2\} \to J_w$ as $k \to \infty$.

$\mu_0^{\tilde{\theta}} = [1, 0, 0]$, $\boldsymbol{x}_{\mathrm{cl}}[0]$ was set to $1_{8\times 1}$ (an 8×1 column vector of ones) and $\boldsymbol{w}[k]$ to 0. To emulate the definition of J_0 (see Definition 3.2) the partial sums $\sum_{l=0}^{k}\|\boldsymbol{y}_{\mathrm{cl}}[l]\|^2$ were computed for each sample path and value of k. The partial sums were then averaged to produce estimates of $\mathbf{E}\{\sum_{l=0}^{k}\|\boldsymbol{y}_{\mathrm{cl}}[l]\|^2\}$. The results are shown in Figure 5 (top). As expected, $\mathbf{E}\{\sum_{l=0}^{k}\|\boldsymbol{y}_{\mathrm{cl}}[l]\|^2\} \to J_0$ as $k \to \infty$. The second simulation set illustrates Theorem 3.3. It is identical to the first simulation set with two exceptions: $\boldsymbol{x}_{\mathrm{cl}}[0] = 0_{8\times 1}$ (an 8×1 column vector of zeros) and $\boldsymbol{w}[k]$ was taken to be zero-mean, Gaussian, i.i.d. process with variance $\sigma_w^2 = 1$. To emulate the definition of J_w in Definition 3.2, the value of $\mathbf{E}\{\|\boldsymbol{y}_{\mathrm{cl}}[k]\|^2\}$ was estimated from the data for every value of k. The simulation results are shown in Figure 5 (bottom). As expected $\mathbf{E}\{\|\boldsymbol{y}_{\mathrm{cl}}[k]\|^2\} \to J_w$ as k grows.

V. Conclusions

The class of dual-random-rate systems, that is, dual-rate systems with a random output (or sensing) rates, has been introduced as a framework to study practical image-based control systems. It was shown that dual-random-rate systems can be reformulated as Markov jump linear systems and analyzed with the tools available for the latter. This point was illustrated through a simulation example: an extended minimum variance controller used to compensate the image drift in a transmission electron microscope. Research is ongoing to extend the dual-random-rate framework to the more general multirate setting.

Acknowledgements

This work is partially carried out as part of Condor, a project under supervision of the Embedded Systems Institute (ESI) and with FEI company as the industrial partner. Condor is partially supported by the Dutch ministry of Economic Affairs under the BSIK program.

References

[1] A. G. Abilov, O. Tuzunalp, and Z. Telatar, "Image-based filtering and control of tubular furnaces," *Automation and Remote Control*, vol. 64, no. 6, pp. 163–174, 2003.

[2] H. Garner, M. Klement, and K. Lee, "Design and analysis of an absolute non-contact orientation sensor for wrist motion control," in *Proc. of the 2001 IEEE/ASME International Conference on Advanced Intelligent Mechatronics*, Como, Italy, 2001, pp. 69–74.

[3] F. Chaumette and S. Hutchinson, "Visual servo control part I: Basic approaches," *IEEE Robotics & Automation Magazine*, pp. 82–90, December 2006.

[4] G. Maimon, A. D. Straw, and M. H. Dickinson, "A simple vision-based algorithm for decision making in flying drosophila," *Current Biology*, vol. 18, no. 6, pp. 464–470, 2008.

[5] D. E. Wyman, B. C. Wilson, and D. E. Malone, "Medical imaging system for feedback control of interstitial laser photocuagulation," *Proc. IEEE*, vol. 80, no. 6, pp. 1069–1082, June 1992.

[6] R. Tsuneta, M. Koguchi, K. Nakamura, and A. Nishida, "A specimen-drift-free EDX mapping system in a STEM for observing two-dimensional profiles of low dose elements in fine semiconductor devices," *Journal of Electron Microscopy*, vol. 51, no. 3, pp. 167–171, 2002.

[7] Q. Yang, S. Jagannathan, and E. W. Bohannan, "Automatic drift compensation using phase correlation method for nanomanipulation," *IEEE Trans. Nanotechnol.*, vol. 7, no. 2, pp. 209–216, 2008.

[8] D. P. Glasson, "Development and applications of multirate digital control," *Proc. IEEE*, vol. 71, no. 11, pp. 2–8, November 1983.

[9] M. C. Berg, N. Amit, and J. D. Powell, "Multirate digital control system design," *IEEE Trans. Automat. Contr.*, vol. 33, no. 12, pp. 1139–1150, December 1988.

[10] A. Tejada, W. Van Den Broek, S. van der Hoeven, and A. J. den Dekker, "Towards STEM control: Modeling framework and development of a sensor for defocus control," in *Proc. 48th IEEE Conference on Decision and Control*, Shanghai, China, 2009, pp. 8310–8315.

[11] D. B. Williams and C. B. Carter, *Transmission Electron Microscopy, A Textbook for Materials Science*. New York: Springer, 2009.

[12] P. Albertos, J. Salt, and J. Tornero, "Dual-rate adaptive control," *Automatica*, vol. 32, no. 7, pp. 1027–1030, 1996.

[13] J. Tornero and M. Tomizuka, "Modeling, analysis and design tools for dual-rate systems," in *Proc. of the 2002 American Control Conference*, Anchorage, AK, 2002, pp. 4116–4121.

[14] G. Xie and L. Wang, "Controllability of periodically switched linear systems with saturating actuators," in *Proc. of the 2004 IEEE International Conference on Systems, Man and Cybernetics*, The Hague, The Netherlands, 2004, pp. 1660–1665.

[15] O. L. V. Costa, M. D. Fragoso, and R. P. Marques, *Discrete-Time Markov Jump Linear Systems*. London: Springer, 2005.

[16] H. Zhang, W. Gray, and O. Gonzalez, "Performance analysis of digital flight control systems with rollback error recovery subject to simulated neutron-induced upsets," *IEEE Trans. Contr. Syst. Tech*, vol. 16, no. 1, pp. 46–59, 2008.

[17] P. M. T. Broersen, "Automatic spectral analysis with time series models," *IEEE Trans. Instrum. Meas.*, vol. 51, no. 2, pp. 211–216, Apr. 2002.

[18] Q. Liang and M. Lemmon, "Robust performance of soft real-time networked control systems with data dropouts," in *2002 IEEE Conference on Decision and Control*, Las Vegas, NV, December 2002.

[19] A. Papoulis and U. Pillai, *Probability, Random Variables, and Stochastic Processes*. New York: McGraw-Hill, 2002, 4th Edition.

[20] Y. Fang and K. A. Loparo, "Stochastic stability of jump linear systems," *IEEE Trans. Automat. Contr.*, vol. 47, no. 7, pp. 1204–1208, July 2002.

[21] W. S. Gray, , H. Zhang, and O. R. Gonzalez, "Closed-loop performance for flight controllers subject to neutron-induced upsets," in *Proc. 42nd Conf. on Decision and Control*, Maui, HI, 2003, pp. 2465–2470.

[22] A. Tejada, O. R. González, and W. S. Gray, "Stability analysis of hybrid jump linear systems with Markov inputs," in *Proc. 46th IEEE Conference on Decision and Control*, New Orleans, LA, 2007, pp. 6280–6285.

[23] A. Tejada, A. J. den Dekker, and W. Van Den Broek, "Introducing measure-by-wire, the systematic use of control theory in transmission electron microscopy," *Ultramicroscopy*, 2011, to appear.

[24] A. Tejada, P. Vos, and A. J. den Dekker, "Towards an adaptive minimum variance control scheme for specimen drift compensation in transmission electron microscopes," in *Proc. of 7th International Workshop on Multidimensional (nD) Systems.*, 2011, to appear.

[25] J. C. H. Spence, *High-Resolution Electron Microscopy, 3rd. Edition*. New York: Oxford University Press, 2003.

[26] G. E. P. Box, G. M. Jenkins, and G. C. Reinsel, *Time Series Analysis: Forecasting and Control*. San Francisco: Holden-Day, 1976.

[27] K. J. Aström, *Introduction to Stochastic Control Theory*. New York: Academic Press, 1970.